Effect of surface state on the catalytic performance of Co/CeO_2 ethanol steam reforming catalyst

Sylwia Turczyniak,[1,2] Detre Teschner,[3] Andrzej Machocki,[2] and Spyridon Zafeiratos[1,*]

[1]*Institut de Chimie et Procédés pour l'Energie, l'Environnement et la Santé (ICPEES), ECPM, UMR 7515 CNRS-Univ. of Strasbourg, 25, rue Becquerel, 67087 Strasbourg Cedex 02, France*

[2] *University of Maria Curie- Sklodowska, Faculty of Chemistry, Department of Chemical Technology, 3 Maria Curie-Sklodowska Square, 20-031 Lublin, Poland*

[3]*Fritz-Haber-Institut der MPG, Faradayweg 4-6, D-14195 Berlin (Dahlem), Germany*

Abstract

This work examines the impact of the Co/CeO_2 catalysts' surface oxidation state and composition on the ethanol steam reforming (ESR) reaction performance. To this purpose, *in situ* and *ex-situ* X-ray Photoelectron Spectroscopy (XPS) combined with *on-line* mass spectrometry were applied at a wide pressure range (0.2 mbar to 20 mbar). When the reaction was performed at 0.2 mbar metallic cobalt and partly reduced cerium oxide was found regardless the catalysts pre-treatment conditions. This surface state favors CO and H_2 production, indicating that C–C bonds cleavage is the most important pathway in this pressure regime. A higher reduction degree of ceria gave rise to a higher population of adsorbed hydroxyl groups, which counterintuitive to the expected behavior, suppressed the activity and the C–C bond cleavage yield. Under higher pressure (4-20 mbar) gradual oxidation of cobalt and ceria was noted. The presence of ionic cobalt species appears to enhance CO_2 and acetaldehyde yields. On the basis of the present results and available literature a plausible, pressure-dependent, reaction mechanism is proposed.

Keywords: Ethanol reforming, ceria, cobalt, reaction mechanism, near ambient-pressure photoelectron spectroscopy.

[*]spiros.zafeiratos@unistra.fr

Graphical abstract

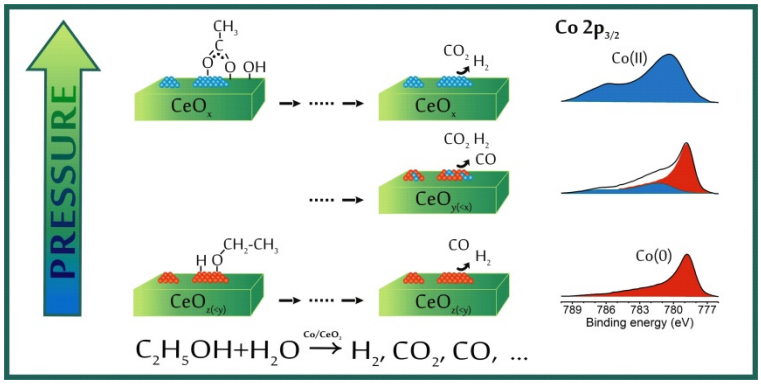

1. Introduction

Increasing demand for energy and concerns about the environmental impact of fossil fuels, call for alternative energy sources and efficient energy carriers. Hydrogen is an ideal energy carrier and, when is produced from sustainable energy sources, has a relatively low environmental impact. Among the possible ways of hydrogen production (i.e. reforming of hydrocarbons, electrolysis, photolytic and biological conversion), the ethanol steam reforming (ESR) seems to be very attractive [1-7]. Cobalt-based catalysts have become one of the most promising ESR catalysts because they have comparable activity with noble metals for C–C bond cleavage in the medium temperatures range, but considerably lower price. Primary disadvantages of cobalt catalysts, such as sintering or deactivation owing to the coke formation, can be limited by selection of a suitable support. From the 70's cerium oxide has emerged as one of the most prominent oxides in catalysis [8] due to its high oxygen storage capacity and its ability to form non-stoichiometric sub-oxides CeO_{2-x} ($0<x<0.5$). It was found that defects in the oxygen lattice of cerium oxide promote CO oxidation [9] and may be activate water in water-gas shift reaction [10, 11].

The effect of ceria particles size on Co/CeO_2 catalysts have been thoroughly investigated by several groups [1, 4, 12-21]. Machocki et al. [12] examined the influence of the support morphology on the catalytic performance and showed that the size of the support particles has an effect on the dispersion of the cobalt active phase and hence, on the catalytic activity and selectivity. The catalyst supported on nano-ceria exhibited 100% ethanol conversion and water conversion close to the stoichiometric (13%). The effect of the support particle size of Co/CeO_2 catalysts in the ESR was also the subject of Soykal et al. [4] research. After hydrogen pre-treatment X-ray Absorption Spectroscopy (XAS) studies showed the presence of almost completely reduced cobalt for the catalyst supported on nano-dispersed ceria and around 88% metallic phase for the catalyst on micro-dispersed ceria. The authors stated that the degree of cobalt reduction is related to the cobalt particles size. In all the above studies high selectivity towards H_2 and CO_2 and low amounts of CO, CH_4, C_2H_4, CH_3CHO were noted. At temperatures below 500°C, severe deactivation of cobalt-based catalyst was observed, leading Wang and co-workers [19] to study the nature of carbon deposit formed during the ESR process. Upon the ESR at 450°C cobalt particles were encapsulated by coke. The deactivation of the catalyst due to coke formation and catalyst encapsulation was assigned to reactions of dehydrogenation and/or dehydratation of ethanol. Some authors [22] suggested that the presence of –OH groups on the surface of Co/CeO_2 facilitate coke-removal.

The nature of the active cobalt phase during the ESR reaction was the focus of studies dealing with unsupported [23-25] and supported [5, 7, 26, 27] cobalt catalysts. The Co_3O_4 spinel phase was not active for the ESR at least in the temperature range of 250 - 350°C [24]. Llorca et al. [23] studied Co_3O_4 transformation during the ESR and observed progressive activation of the sample under the reaction feed. Initially, on the oxidized sample, hydrogen and acetaldehyde were the major products but after 2 h of reaction at 400°C, activation of cobalt occurred, and almost 100% conversion of ethanol to H_2 and CO_2, was achieved. In the *operando* XRD study of de la Pena et al. it was found that a mixture of both CoO and metallic Co phases was active and very selective in the ESR reaction [25]. However, numerous other publications assumed that the metallic cobalt is the most active form of cobalt in the ESR [27-29] even if in some cases, promotes catalyst deactivation [30]. Recently, the idea that different cobalt oxidation states might favor different reaction paths is gaining ground. Metallic cobalt is associated to ethanol decarbonylation to CO and CH_4 [30], or formation of the acetaldehyde [31, 32], while ionic Co^{2+} sites seems to be responsible for selective oxidation of ethoxide species to acetaldehyde [33]. However, Bayram et al. [34] showed that under the ESR CO_2 and H_2 were the major products even if both forms of cobalt Co^0 and Co^{2+} were present.

Although the crucial role of cobalt and ceria surface state during the ESR reaction is recognized, definition of the chemical state of the active catalyst remains a key challenge. Reliable information can be provided when the surface characterization of the catalyst under working ESR conditions is combined with the evaluation of the catalytic performance. In this work the Co/CeO_2 ethanol steam reforming catalyst was analysed *in-situ* by synchrotron based XPS and absorption spectroscopies combined with *on-line* mass spectrometry. To account for the pressure limits of this method the *in-situ* results are completed with higher pressure XPS studies where the working catalyst is quenched by rapid exposure to vacuum conditions. These findings reveal some new insights about the role of ceria and cobalt in the ESR reaction.

2. Experimental Section

The Co/CeO_2 catalyst was prepared by the impregnation method. The commercial nano-dispersed ceria support (Aldrich) was initially dried at 120°C for 3 h and consequently impregnated with a 1/1 molar cobalt nitrate and citric acid solutions. After impregnation, the catalyst precursor was dried at 120°C for 12 h and then calcined at 400°C for 1 h.

The *in-situ* synchrotron-based X-ray photoelectron (*in situ*-XPS) and absorption spectroscopies (XAS) were performed at ISISS beamline at BESSY in Berlin, in a set-up described in details elsewhere [35]. The soft X-ray absorption spectra of the Co $L_{3,2}$ and Ce $M_{4,5}$ edges were recorded in the Total Electron Yield (TEY) mode. The gas phase composition was monitored *on-line* by a differentially pumped quadrupole mass spectrometer (QMS), which was connected to the experimental cell through a leak valve. The catalyst was initially pre-treated in the XPS cell in oxygen (0.2 mbar O_2 at 250°C) to remove all residual surface carbon. A similar procedure was repeated after each reaction cycle to "refresh" the surface and eliminate carbon deposit as confirmed by C 1s XPS spectrum. The ESR reaction was performed in several cycles at the same catalytic specimen under identical reaction conditions. Prior to any reaction cycle the sample was treated in reducing (0.2 mbar H_2 at 250°C or EtOH at 420°C) or oxidative (0.2 mbar O_2 at 250°C) environments. The aim of this pre-treatment was to induce modifications at the catalysts' surface state during the subsequent ESR reaction cycle. This is feasible since the kinetics of surface transformation under the reaction mixture are relatively slow, allowing for different surface states to maintain for periods comparable to the XPS acquisition time (e.g. 30 min). In this way under reaction conditions the predominant bulk characteristics of the catalysts remain similar while the surface state might vary considerably [36].

The ethanol/water mixture (1/3 mol/mol) with an overall pressure of 0.2 mbar was introduced after cooling down the sample to 50°C. Consequently the sample was heated to 420°C (by 5 C min^{-1}), and spectra were recorded after about 15 min, where QMS signal showed a stable catalytic performance. Spectra were recorded using appropriately selected photon energies, resulting in photoelectrons with two characteristic kinetic energies (180 and 465 eV) and therefore two different analysis depths (ca. 1.7 and 2.9 nm). Quantitative calculations were performed taking into account the photon-energy dependence of the atomic subshell photo-ionization cross-sections.

The *ex situ* laboratory-based XPS measurements were carried out in an ultrahigh vacuum (UHV) setup combined with an attached variable-pressure 0.6 *l* reactor (VPR). The analysis chamber of the UHV setup is equipped with a hemispherical electron analyzer and a dual X-ray source. The AlKα line at 1486.6 eV was used for the *ex situ* XPS measurements. The powder sample was pressed into a 13 mm pellet and mounted on a sample holder with boron nitrate heater and a temperature sensor attached to it, which can be used both in UHV and VPR chambers. The gas inlet and gas detection systems were analogous of those in the

synchrotron-based XPS setup. Prior to the reaction the samples were reduced in hydrogen (10 mbar) at 420 °C during 1h and then exposed to the reaction mixture at various pressures. Catalytic experiments in the VPR chamber were performed in 3 distinct pressure regimes, namely 4, 10 and 20 mbar. After about 30 min under ESR reaction conditions at 420°C, the state of the reacting surface was quenched by cooling down rapidly and pumping off the gas mixture ($p<1x10^{-7}$ mbar) from the VPR chamber. Consequently the sample was rapidly transferred under UHV from the reactor to the analysis chamber for XPS characterization.

The conversion of EtOH and H_2O under the ESR conditions was calculated from the change of QMS EtOH ($m/e = 31$) and H_2O ($m/e = 18$) intensities. The product yields were calculated by the increase of the H_2 ($m/e = 2$), CO ($m/e = 28$), CH_3COH ($m/e = 29$) and CO_2 ($m/e = 44$) QMS intensities induced by the catalytic reaction. A correction of the ion current signals due to fragmentation was also taken into account. Since QMS signals were not calibrated to the sensitivity factor of each gas, the product yields are used in a % comparative basis and therefore described as relative (products) yields. For more details about the calculation method of conversion and the product yields please refer to *supporting information* 1. The blank experiment, performed under mbar conditions for the $EtOH/H_2O = 1/3$ mol/mol showed low ethanol and water conversions which do not exceed 20% of those found with the catalyst loaded in the reactor. The contribution of the background conversion was taken into account during the QMS data processing.

Transmission electron microscopy images were obtained with the FEI Titan G2 60-300 kV microscope at an electron beam accelerating voltage of 300 kV. Elemental mapping was carried out in the scanning transmission electron microscopy (STEM) mode by collecting point by point Energy-dispersive X-ray spectra (EDS) at each pixel in the map. More details about the experimental procedure followed in this paper can be found in *supporting information* 1.

3. Results

3.1 Textural and morphological characteristics of the fresh catalyst

Table 1 shows structural characteristics of the ceria support and the cobalt-ceria catalyst. The total surface area of the CeO_2 support was about 73 m^2/g and after cobalt deposition decreased slightly to 67 m^2/g. The average size of CeO_2 particles increased from 22 to 30 nm after cobalt deposition, as calculated on the basis of XRD results. The absence of cobalt-related peaks on the XRD pattern suggests highly dispersed cobalt oxide on the

support. The average cobalt crystallite size (in the reduced catalyst) as calculated on the basis of hydrogen chemisorption measurement was about 14 nm.

Table 1.
Support and catalyst textural characterization results.

	Pore volume (cm^3/g)	**Pore diameter (nm)**	**Total surface area (m^2/g)**	**Support crystallite size (nm)[a]**	**Co content (wt.%)**	**Cobalt surface area (m^2/g)**	**Average cobalt crystallite size (nm)[b]**
CeO_2	0.331	14.2	72.9	22	-	-	-
Co/CeO_2	0.191	8.8	66.9	30	7.9 ± 0.3	3.82	14.0

[a] On the basis of the XRD measurements.
[b] On the basis of hydrogen chemisorption measurements.

Prior to the XPS measurements the morphology of ceria support and cobalt/ceria catalyst was examined by AFM, STEM, and STEM-EDS methods. In general, cobalt deposition did not change significantly the morphology of the support (see *supporting information 2*). The average ceria crystallite size for the Co/CeO_2 calculated from TEM images (see *supporting information 2*) was 24.5 nm close to the result obtained from the XRD measurements (30 nm). The difficulty in distinguishing between ceria and cobalt oxide crystallites in the TEM images suggests that cobalt is well-dispersed on the support and does not form large aggregates. This is further supported by EDS mapping of Ce, Co and O in the STEM mode (STEM-EDS) shown in Fig. 1. From the compositional image it can be seen that the distribution of cobalt oxide on the support is almost homogenous, with rare agglomerates. Although microscopy images were obtained from catalyst already calcined at 400 °C, one cannot exclude that the morphological characteristics are modified under the reaction conditions. However, it is recognized that the state of the ESR catalyst prior to the reaction has a notable impact on the catalytic behavior [15].

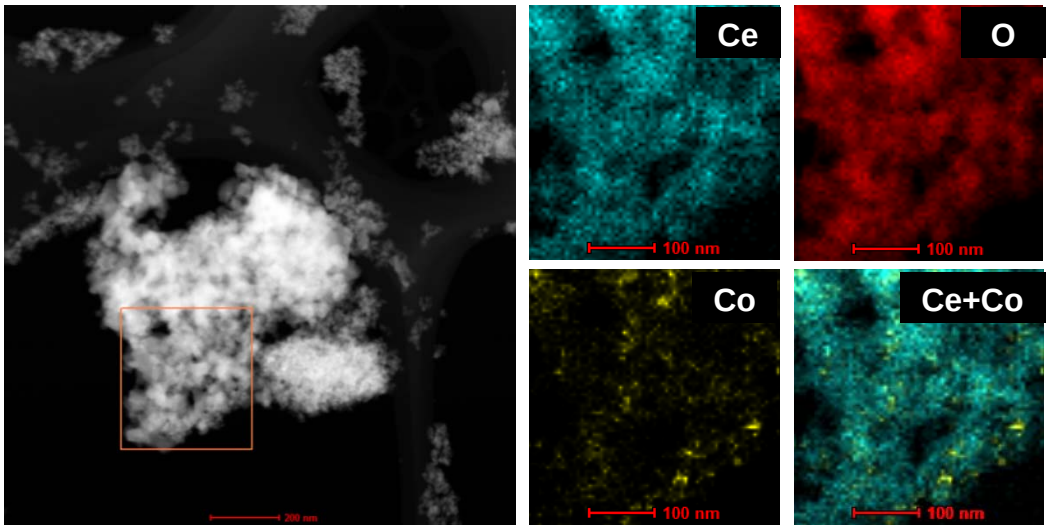

Fig 1. STEM image with selected area mapping and STEM-EDS spectrum images showing the elemental composition of calcined Co/CeO_2 catalysts.

3.2 The Co/CeO_2 oxidation state under the ESR reaction at 0.2 mbar

Before the ESR reaction the Co/CeO_2 catalyst was conditioned in the spectrometer under oxidative (O_2) or reductive (H_2 or ethanol vapor) gas phase environments. Fig. 2a and b show the Ce 3d and Co $2p_{3/2}$ synchrotron-based XPS spectra recorded during the various pretreatment atmospheres and the following-up ESR reaction. In O_2 the Co $2p_{3/2}$ peak at 779.7 eV (bottom spectrum) is assigned to the Co_3O_4 spinel phase [37], as also confirmed by the Co L_3-edge XAS spectrum shown in *supporting information 3* [36, 38-40], while the Ce 3d peak corresponds to CeO_2 [41-42] (Fig. 2b). In reducing pretreatment conditions (0.2 mbar H_2 or ethanol vapors at 420°C) cobalt is fully reduced to the metallic state (Co^0) as shown by the characteristic Co 2p peak at 778.3 eV, while ceria is partially reduced to a mixture of Ce(III) and Ce(IV) (Fig. 2a and b). Please note that in EtOH atmosphere the background of the Co $2p_{3/2}$ spectrum is perturbated due to severe carbon deposition as will be discussed below. However the Co L-edge spectrum presented in *supporting information 3*, confirms the metallic state of cobalt. In addition the differences in the Ce 3d spectra suggest that ceria is more reduced in ethanol atmosphere as compared to H_2.

During the ESR reaction ($EtOH/H_2O$ = 1/3 mol at 420°C) the Co $2p_{3/2}$ photoemission (Fig. 2a) and Co $L_{3,2}$-edge XAS spectra (see *supporting information 3*) [40] are characteristic of metallic Co^0, independently of the prior surface state under the pretreatment atmosphere. On the other hand, in agreement with previous reports [41], the Ce 3d spectrum corresponds to partially reduced ceria composed by a mixture of Ce(III) and Ce(IV) oxides (*see Table 2*) [42-45]. In contrast to cobalt, the exact valence of ceria does influenced by the pre-treatment,

as indicated by the small but notable differences in the Ce 3d spectra. It is also interesting to note that similar oxidation states of Co and ceria were observed even if the pre-treated catalyst was exposed in the ESR mixtures with H_2O excess (1/8 mol/mol) (*data not shown*), showing that the mixing ratio has limited effect on the oxidation state under these conditions.

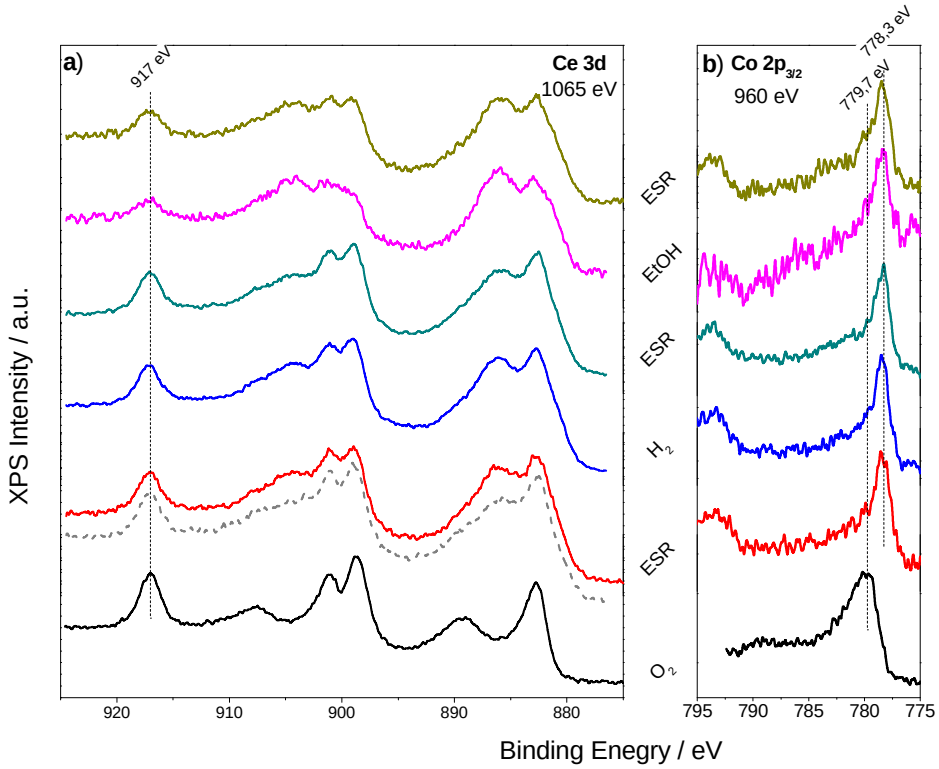

Fig. 2. *Synchrotron-based* XPS (a) Ce 3d (*hv* = 1065 eV) (b) Co $2p_{3/2}$ (*hv* = 960 eV) spectra of the Co/CeO_2 catalyst in (*from bottom to the top*): O_2 at 250°C, subsequent ESR reaction (2 experiments with different O_2 pre-treatment duration), H_2 at 420°C, subsequent ESR reaction, EtOH at 420°C, subsequent ESR reaction. The ERS reaction condition were $EtOH/H_2O$ = 1/3 mol/mol at 420°C and the overall pressure was 0.2 mbar.

The quantitative analysis of the XPS spectra provides information about the surface composition under the ESR conditions. In the results presented in Table 2 the Co 2p to Ce 3d atomic ratio was used in order to estimate relative modifications on the cobalt surface distribution, while spectra from different analysis depths can indicate possible surface segregation or layered structure. Please note that even if the ESR reaction mixture modifies the oxidation state compared to the pretreatment, the slow kinetics of ceria modification, induce a "*memory effect*" on the catalyst and helps to maintain different ceria oxidation states under ESR. The percentage contribution of Ce(III) was determined after deconvolution of Ce 3d spectra into Ce(III) and Ce(IV) components. This was done for spectra recorded using two excitation photon energies and thus two information depths (EK_1 = 180 eV [information depth

~1.7 nm] and EK_2 = 465 eV [~2.9 nm]) (*supporting information* 4). As shown in Table 2 reduced ceria is systematically enhanced at the lower analysis depth, indicating that there is a gradient of Ce^{3+} species from the surface towards the interior. In addition, the pre-treatment of catalysts in pure oxygen, hydrogen or ethanol did not have a significant effect on the measured Co/Ce atomic ratio under the ESR, suggesting that the pretreatment has limited influence on the surface composition during the ESR reaction. Finally, comparison of the Co/Ce peak area ratio in the two analysis depths does not show substantial differences. Accordingly one can rule out extended surface segregation phenomena and propose homogenous mixing of cobalt and ceria in the outer 3 nm of the catalyst. Overall, our results reveal that under the ESR conditions the surface oxidation state and composition of the catalyst adapts primarily to the ESR reaction mixture and is moderately influenced by the prior oxidation state.

Table 2: The percentage of Ce (III) species as well as the Co/Ce and C/(Ce+Co) surface atomic ratios obtained by *in-situ* synchrotron XPS measurements of Co/CeO_2 catalyst during ESR. Prior to the reaction the catalyst had undergone different pre-treatments in O_2, H_2 or EtOH. Spectra were measured using selected photon energies, so as to obtain measurements at two different information depths (i.d.).

Pre-treatment	Ce(III) (%)		Co/Ce*		C/(Ce*+Co)
	i.d.** 1.7 nm	2.9 nm	1.7 nm	2.9 nm	1.7 nm
O_2 250°C(1)	41.6	28.3	0.15	0.18	0.10
H_2 420°C(2)	44.9	33.4	0.15	0.16	0.02
O_2 250°C(3)	51.1	37.7	0.14	0.16	0.02
EtOH 420°C(4)	64.1	43.5	0.17	0.18	3.36

*Ce = Ce_2O_3+CeO_2, **Estimated information depth, (1)Pre-calcined sample treated at the indicated conditions for 60 min, (2)Sample treated at the indicated conditions for 30 min, (3)Pre-reduced sample treated at the indicated conditions for 10 min, (4)Sample treated at the indicated conditions for 10 min.

The O 1s and C 1s core level spectra recorded during ESR reaction on samples which were subjected to different pre-treatments are shown in Fig. 3. Analysis of the O 1s peak indicate three O 1s components at 530.0, 531.2 and 533.0±0.1 eV due to ceria lattice oxygen (O_{lat}), adsorbed hydroxyl [7, 46-48] and water [46-48] species respectively (the addition of both hydroxyl and water species is abbreviated as OH_{ads}). Please note that the O 1s components at 533 eV has been also assigned to surface lattice defects [49, 50], however this is less likely here since the relative intensity of 533 eV component is not increasing for more reduced samples. The C 1s region (Fig. 3b) recorded under ESR conditions shows a broad peak at 289.5 eV due to the Ce 4s core level and a peak at 284.8±0.2 eV typically assigned to

graphite and/or C=C [51, 52] and $-CH_x$ species [53]. Oxygenated carbon species (e.g. CO_3^{2-} [54]) are not observed and therefore their contribution to the O 1s spectra should be excluded.

The relative amount of O_{lat} and OH_{ads} species can be estimated from the O 1s peak analysis and combined with the ceria oxidation state (Ce(III)) as shown in Fig. 3c. As expected, the O_{lat}/Ce ratio decreases when ceria is reduced, while the OH_{ads}/*Ce* ratio increases, with the only exception of the state in which severe carbon deposition occurred (Ce(III) ca. 62%). The increase of relative amount of OH_{ads} species with parallel reduction of ceria suggests the partial replacement of ceria lattice oxygen by OH_{ads} species formed due to water and/or ethanol dissociation. In addition, the drastic reduction of OH_{ads} upon severe carbon deposition indicates that adsorbed carbon and OH_{ads} species compete for the same adsorption sites on the ceria surface. Please note that the O_{lat}/Ce stoichiometry shown in y-axis of fig. 3c is systematically higher than that expected from the Ce(III) value. This might be an effect of systematic errors in the O_{lat}/Ce calculations arising from uncertainties at the sensitivity factors and the O 1s deconvolution procedure. However, the trend between O_{lat}/Ce stoichiometry and Ce(III) species is consistent in both cases implying the reduction of ceria.

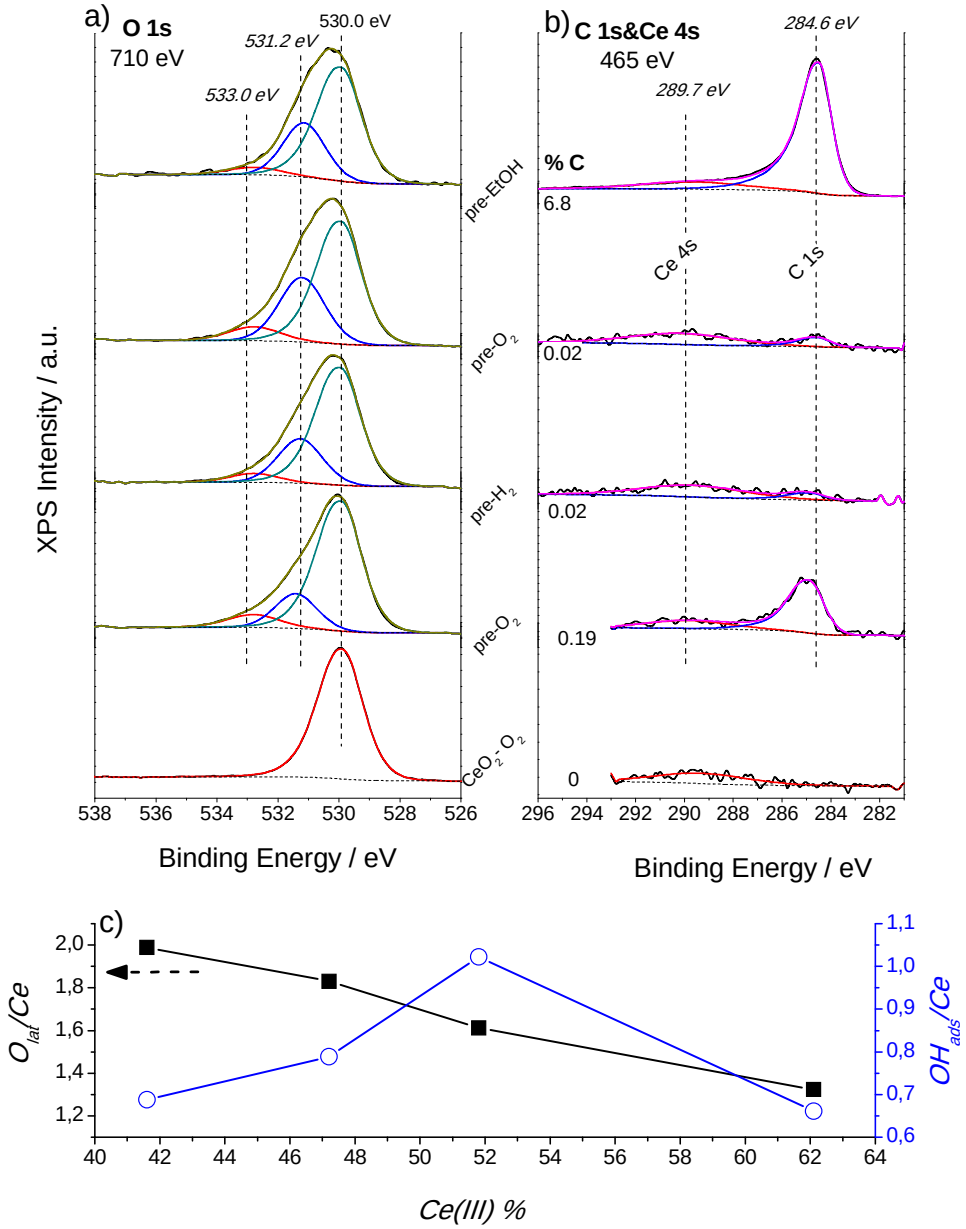

Fig. 3. *Synchrotron-based* XPS (a) O 1s (hv= 710 eV) and (b) C 1s & Ce 4s (hv= 465 eV) core level spectra during the ESR reaction (EtOH/H_2O = 1/3 mol/mol at 420°C, p = 0.2 mbar) over Co/CeO_2 samples undergone different pretreatments. Reference spectra recorded on pure CeO_2 under oxidative atmosphere are shown at the bottom. (c) The evolution of the lattice (O_{lat}) and adsorbed (OH_{ads}) oxygen species acquired after the O 1s peak deconvolution as a function of the percentage contribution of Ce(III) species in the overall Ce 3d spectrum.

3.3 Correlation of the surface state with the catalytic conversion and the products yield

Having shown the correlation of ceria oxidation state with the population of the adsorbed oxygen species, it is interesting to investigate its effect on the activity and selectivity of the catalyst. By means of *on-line* QMS analysis, mass fragments due to reactants and potential products of the ESR reaction, were recorded. The activity of the catalyst is

demonstrated by the consumption of ethanol and water, as well as by the detection of mass fragments due to various reaction products (*supporting information 5*). Taking into consideration the blank experiment and after fragment correction four main reaction products are detected in the gas phase, namely H_2 (m/e=2), CO (m/e=28), CO_2 (m/e=44) and CH_3CHO (m/e=29). Due to the particular conditions of the experiments other products like CH_4 (m/e=16), acetone (m/e=43), or ethylene (m/e=27), etc. typically referred as ethanol steam reforming byproducts, if present, were below the detection limit of *on-line* gas phase analysis.

In Fig. 4a and 4b we present the conversion of ethanol (m/e=31) and water (m/e=18) recorded by *on-line* mass spectrometry as a function of Ce(III) percentage and the relative abundance of OH_{ads}, (*OH*/(*Co*+*Ce*)) obtained from the *synchrotron-based* XPS. Both ethanol and water conversions are enhanced on more oxidized ceria substrate (Fig. 4a), while the population of OH_{ads} groups has the reverse effect. As mentioned above (Fig. 3c) carbon deposition limits the relative abundancy of OH_{ads} species and probably replaces them with hydrocarbon species. This can explain why the liner correlation between EtOH and water conversion with OH_{ads} is perturbated in the case of severe carbon deposition (Fig. 4b). However, evidently the influence of carbon deposit on the H_2O conversion is less as compared to that of EtOH conversion.

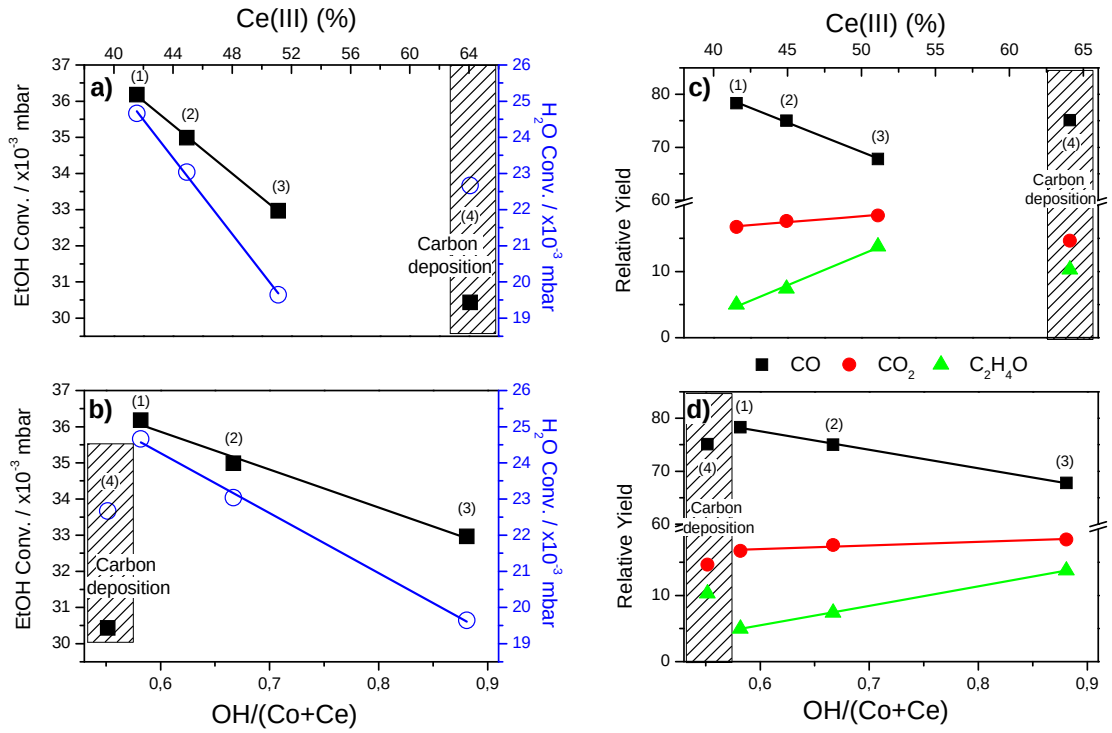

Fig. 4. (a) Correlation of the % Ce(III) fraction to the overall ceria (b) the relative amount of adsorbed hydroxyl species (OH/*(Co+Ce)*), with ethanol and water conversion. (c) Correlation of the % Ce(III) fraction to the

overall ceria and (d) the relative amount of adsorbed hydroxyl species (OH/*(Co+Ce)*), with carbon products yields (the ESR reaction conditions 420ºC, 0.2 mbar C_2H_5OH : H_2O = 1:3 mol/mol). The % Ce(III) and OH/*(Co+Ce)* values were obtained from synchrotron-based XPS spectra with estimated information depth 1.7 nm. The dashed areas highlight ESR reaction on samples with severe carbon deposition. Each point represents reaction performed after different pretreatment of the Co/CeO_2 catalyst. The numbers in parenthesis correspond to the treatment before ESR reaction: [(1)]Pre-calcined sample treated at 250 ºC in O_2 for 60 min, [(2)]Sample treated at 420 ºC in H_2 for 30 min, [(3)]Pre-reduced sample treated at 250 ºC in O_2 for 10 min, [(4)]Sample treated at 420 ºC in EtOH for 10 min.

In Fig. 4c and d the relative yield of each carbon product is presented as a function of % Ce(III) and the amount of adsorbed species. The relative yield of CO_2 is practically independent of the oxidation state of ceria and the amount of adsorbed oxygen species. However, CO and acetaldehyde show an opposite tendency. In particular, CO is enhanced as ceria becomes more oxidized and the amount of OH_{ads} species decreases, while acetaldehyde shows the reverse trend.

3.4 Effect of the reaction pressure on the oxidation state and the product selectivity

As shown above during the *in situ* synchrotron-based XPS experiments relatively high yield to CO was observed, which was not the case when the catalyst was tested in a flow fixed-bed reactor at atmospheric pressure [2]. In addition, metallic cobalt was always the valence state observed under the employed ESR reaction conditions (even in water-rich mixture), while in the past several authors gave evidences for the presence of oxidized cobalt species. Therefore a justified question is whether the high CO yield and metallic Co observed at the low pressure XPS experiments are interrelated. Accordingly the ESR reaction was performed up to two orders of magnitude higher pressure in a combined high-pressure reactor/UHV set up, which allowed the characterization of the catalyst just after reaction without exposure to air. Samples from the same batch were pre-reduced in the reactor at 420°C in H_2 prior to the ESR reaction. Apart from the overall pressure, care was taken that the other reaction conditions (pre-treatment, temperature, $EtOH/H_2O$ mixing ratio and reaction time) are identical to those of the synchrotron studies. The Co $2p_{3/2}$ and Ce 3d spectra indeed indicated that the reaction pressure has a prominent effect over the surface oxidation state (see fig. 5). Increasing the ESR reaction pressure enhances oxidation of cobalt and ceria. Although a post reaction re-oxidation of cobalt by residual water in the high pressure reactor cannot be excluded, there is a clear trend between the cobalt oxide formation and the reaction

pressure, allowing linking the low pressure *synchrotron-based* XPS experiments with the real ESR conditions.

In Fig. 5e we present the product yields as a function of the reaction pressure (from 0.2 to 20 mbar) and the cobalt and ceria oxidation state. From the graph, it is clear that as the reaction pressure increases from 0.2 to 20 mbar cobalt and ceria are gradually oxidized. This has also a direct effect on the carbon product selectivity with CO gradually replaced by relatively higher CO_2 and acetaldehyde production. Please note that in the synchrotron XPS experiments of Fig. 4c, the CO yield drops with the increase of Ce(III) species, which is the reverse trend as compared to the pressure-dependent experiments of fig. 5d. This discrepancy can be explained by the differences in the oxidation state of cobalt observed in the two cases. In particular at low pressure experiments (fig. 4c) cobalt is metallic, while at higher pressure (fig. 5d) cobalt is partly oxidized. Since the catalytic performance depends both on the ceria and cobalt oxidation states, one can anticipate that differences in the cobalt oxidation state will have a prominent effect on the ESR products. This argument can qualitatively explain the differences in the various pressure regimes and confirm that the catalytic performance is a complex interplay between ceria and cobalt oxidation states.

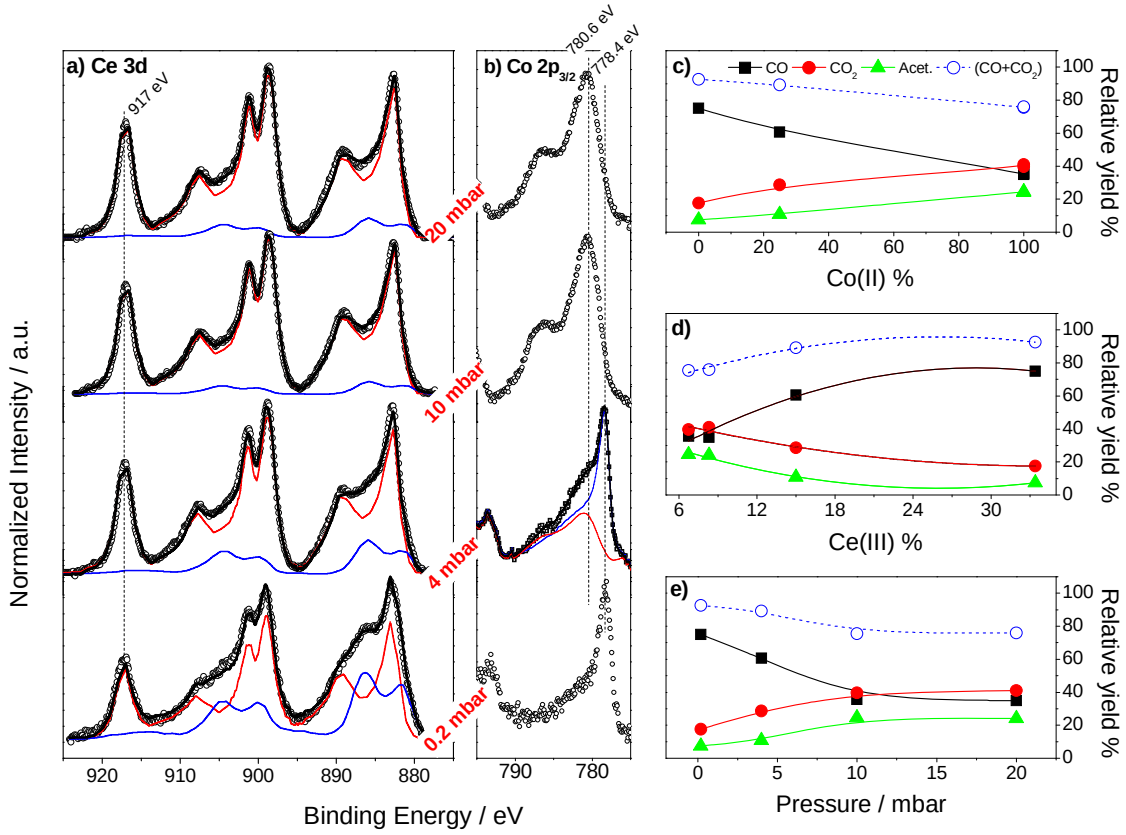

Fig. 5. (a) Ce 3d and (b) Co $2p_{3/2}$ XPS spectra recorded over Co/CeO_2 catalysts after the ESR reaction ($EtOH/H_2O$ = 1/3 mol/mol at 420°C) at different pressure regimes (p = 0.2- 20 mbar). The bottom XPS spectra are recorded *in situ* at a synchrotron setup (using hv = 1350 and 1245 eV), while higher pressure results are *ex-situ* from a high-pressure reactor attached to UHV set up using an AlKα source. The product yields are obtained by the QMS analysis as a function of (c) Co(II) (d) Ce(III) and (e) reaction pressure. Please note that the Ce(III) and Co(II) % at 0.2 mbar (synchrotron-XPS) was calculated from spectra recorded using 1350 and 1245 eV excitation photon energy.

It is very difficult to determine the effect of overall pressure on the product selectivity, since the Co/CeO_2 adapts fast its oxidation state to the ESR mixture pressure. Nevertheless, fig. 5 shows that there is a net monotonic correlation between the oxidation states of ceria and cobalt and various products, which is a very important fact for the ESR reaction.

4. Discussion

4.1. Effect of the surface state to the conversion of ethanol and water

The results of Fig. 3c evoke that reduction of ceria during the ESR reaction is accompanied by the replacement of lattice oxygen from adsorbed oxygen species (mainly OH groups), in accordance with previous reports [51]. Since the oxidation state and the relative amount of cobalt are stable, the drop of EtOH and H_2O conversion can be correlated with the decrease of the oxidation state of ceria which induces a collateral increase of adsorbed oxygen species (Fig. 4). Therefore, contrary to the common conception, adsorbed OH groups are not promoting, but rather inhibiting, the ESR reaction under low pressure conditions. This inhibitory effect should be explained by the occupancy of adsorption sites by strongly bounded, stable OH species, which are unable to participate in ethanol transformations. On the other hand, the abundance of ceria lattice oxygen species (ca. 530 eV in O 1s spectrum) is evidently promoting the catalytic conversion. It can be also seen in Fig. 4b that carbon deposition drastically reduces the amount of OH_{ads} species suppressing primarily ethanol conversion, and to a less extent, water conversion. This observation indicates that the mechanism of water and ethanol activation involves, to some extent, different surface sites.

4.2. Effect of the surface state to the ESR reaction products yield

The correlation between experiments at the various pressure regimes may be used to propose the pressure-dependent reaction scheme shown in Fig. 6. Literature does not provide a direct answer on the nature of active species under the ESR [33, 55] however, it is often

assumed that metallic cobalt is the active site [25-27, 29, 31, 56]. Therefore, the adsorption of ethanol (as ethoxy species) on metallic particles [30, 57] is considered as the initial step of EtOH transformation (1) [31, 58]. Ethanol, similar to other alcohols also dissociatively adsorbs on ceria [7, 59, 61] however, studies of I.I. Soykal et al [4, 62] and H. Song et al [16] have shown that bare ceria exhibits rather poor activity in C-C bonds cleavage in temperature range of 400-450°C. Studies of A.M. de Silva suggest that EtOH conversion ~50% can be achieved at 500°C with $EtOH/H_2O = 1/3$ mol/mol [61, 63]. Therefore, metallic cobalt particles were considered as the most significant EtOH adsorption sites in the proposed mechanism. As for H_2O activation, it is expected that it occurs mainly on cobalt particles and either forms a oxidized cobalt layer or transfer to the support and reduce ceria to Ce(III). Recent DFT studies [64] suggest that water dissociation is strongly promoted on Co nanoparticles, meaning that water can be easily converted into atomic O releasing H_2. Furthermore, ceria lattice oxygen can spillover to cobalt [33]. If this oxygen layer is very thin and do not induce modifications at the Co 2p spectrum, it will be difficulty detectable by XPS, but it will still influence the catalyst selectivity [65]. Since there is no evidence of cobalt oxidation at 0.2 mbar and cobalt dispersion is high, it can be assumed that in that case most of –OH species are located on the support surface.

The adsorbed ethoxy species can undergo scission of the Cα–H bond (2) and desorbs as CH_3CHO (3) [30, 66, 67] or undergo C–C bond scission [66] which will lead to CO and/or CO_2 [30] (please recall that CH_4 production was negligible here) with parallel H_2 production. Results in fig. 5 indicate interdependence between $CO+CO_2$ and CH_3CHO yields suggesting that these products are formed by two antagonistic reaction paths. As mentioned before, ceria itself can also participate in EtOH and H_2O transformations [4, 61-63, 68] and influence the reaction pathways. Some authors highlight ceria importance, whereas the role of metal particles is rather diminished [21, 61, 63, 69], even though unsupported cobalt was found to be very selective in the ESR [25, 70]. We suggest that the main role of ceria at low pressure is to provide mobile oxygen to cobalt-ceria interface [33]. High reduction degree of ceria may led to formation of C_2H_4 which is well known coke precursor [51, 71]. This can be supported by the decrease of CO_2 formation and increase of the mass signal 28 which can be ascribed to CO and C_2H_4.

At low pressure experiments (0.2 mbar) CO is the major product; therefore the cleavage of C–C bonds is proposed as the most favourable pathway (4-10), what is in agreement with the studies of H.P. Hyman et al [30]. The negligible amounts of CH_4 can be

explained by scission of C–H bonds leading to C deposition (8) [61, 63, 66], which is subsequently oxidized by water (9-10) [61, 63], since carbon deposition was limited over catalysts pre-treated in O_2 or H_2. Fig. 4d shows that the abundance of adsorbed oxygen species enhances the yield of CH_3CHO in the expense of CO, even if CO_2 production remained practically constant. Therefore, at 0.2 mbar, further oxidation of CO to CO_2 is suppressed, despite a considerable amount of adsorbed OH groups indicated by the XPS results. Formation of CO_2 under examined conditions can be a result of the presence of a surface layer of adsorbed oxygen containing species (e.g. in form of –OH species or atomic O). Studies of E. Martono et al [65] suggest that even if cobalt remains predominantly metallic, some oxygen adlayer may exist and influence CO_2. In agreement L. De Rio et al [70] suggest that CoO_x phase is required in order to obtain sufficient CO_2 selectivity. At higher pressure (4-20 mbar) ESR reaction on Co/CeO_2 catalysts proceeds mainly through the formation of acetate species (CH_3COO–), as has been reported based on *in situ* DRIFT studies [17, 34, 31]. This pathway is possible due to the presence of oxidized cobalt (12-14) and weakly bonded –OH species on the support (16-18). The transformation of ethoxy species to acetate in the presence of CoO has been previously suggested in literature [34]. The transformation of $–CH_3$ species advance through pathways (14) and/or (7-10) [61, 63]. One should clarify that the proposed reaction steps are the main reaction pathways in each pressure without excluding a lesser participation of the other steps.

The relatively high concentration of CO among C-containing products can be rationalized taking into account the influence of the pressure on the chemisorption properties of the catalyst surface. In general two main sites responsible for reagents chemisorption can be distinguished *(i)* strong adsorption sites, such as low-coordinated centres (corners, edges, lattice defects) and *(ii)* weak sites, such as terraces on the crystallites surface. It is well known that depending on the reaction conditions, adsorbed oxygen-containing species can be spectators, inhibitors or they can facilitate some reaction pathways. Usually, as a first step of the ESR, ethanol adsorption (mainly on metal particles) and water (dissociation on metal and ceria support) are considered [66, 72, 73]. At very low pressure, chemisorption from the gas phase occurs preferentially on the strong chemisorption centres, while with the increase of the pressure also weak centres are populated and involved in the ESR reaction. Strongly chemisorbed species restrain mobility (diffusion) over the surface, therefore there is a lower possibility to react with other species. In addition, further dissociation of ethanol and water will be inhibited, due to occupancy of the absorption sites.

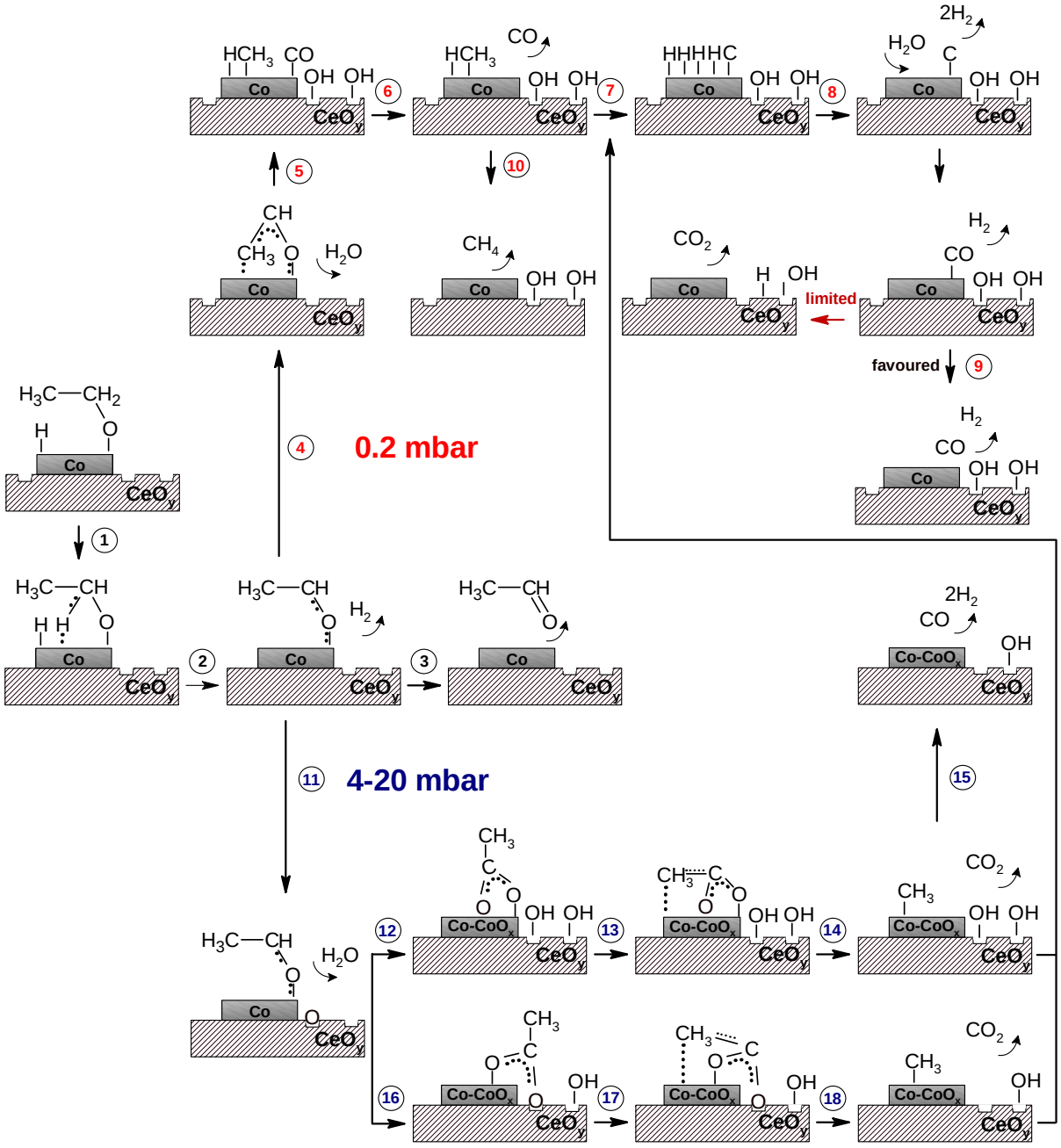

Fig. 6. Proposed reaction paths of ESR reaction over Co/CeO_2 catalyst in various pressure regimes. For clarity of the scheme, -OH species adsorbed on cobalt surface are omitted.

The *ex situ* studies performed at higher reaction pressure (4-20 mbar) show the enrichment of the surface with Co^{2+} and Ce^{4+} species, with parallel increase of the yield towards CO_2 and CH_3CHO (Fig. 5). The increase of CH_3CHO yield is not surprising since ionic Co^{2+} is known to be less active in C–C bonds cleavage than metallic Co [30, 74]. Further transformation of formed acetaldehyde may presumably proceed on cobalt-ceria interface. Studies have shown that depending on both: morphology and oxidation state, ceria

may exhibit different performance toward acetaldehyde transformations. [51, 75] Acetaldehyde reacts on oxidized CeO_2 (100) producing CO_2, CO and H_2O as primary products, while on reduced CeO_2 (100) surfaces it forms mainly H_2 and C. However, even at the elevated reaction pressure (20 mbar) substantial amount of CO was present within the products. Therefore one cannot exclude the existence of metallic Co species under the ESR conditions [76], which do not withstand the sample transfer to the analysis chamber and oxidize. Higher CO_2 yield can be assigned both to the presence of Co^{2+} species [70] and to more reactive/mobile –OH groups on the support and cobalt as well.

Conclusions

A high surface area Co/CeO_2 catalyst prepared by impregnation method was investigated using combined *in situ* and *ex situ* XPS in seeking to understand the implications of the surface state to the ESR catalytic performance. It was found that the active surface state is formed primarily under the ESR reaction mixture and the catalytic pretreatment has a limited effect on the surface characteristics. In the presence of metallic cobalt and reduced ceria CO production is favored, while ionic cobalt species promotes CO_2 and CH_3CHO yields. A higher population of adsorbed hydroxyl groups is build up with the reduction degree of ceria however, under the examined low pressure conditions, hydroxyl groups' act more as inhibitors rather than promoters of the ESR reaction rate. Finally, at constant cobalt oxidation state, the cleavage of C–C ethanol bond is favored on more oxidized ceria supports.

Acknowledgement

S.T. acknowledges support from Campus France, PHC Polonium, Project No. 27700SJ. The research leading to these results has received funding from the European Community's Seventh Framework Programme (FP7/2007-2013) under grant agreements n.312284 and n.226716. We thank G. Słowik from University of Maria Curie-Sklodowska in Lublin for his help with the microscopic studies which were carried out at an equipment purchased thanks to the financial support of the European Regional Development Fund in the framework of the Polish Innovation Economy Operational Program (contract no. POIG.02.01.00-06-024/09 Center of Functional Nanomaterials). Finally, we acknowledge the Inorganic Chemistry department of the Fritz-Haber- Institut der MPG, in particular M. Hävecker and A. Knop-Gericke for the opportunity to use ISISS beamline and HZB for the allocation of synchrotron radiation beamtime.

References:

1 P. Rybak, B. Tomaszewska., A. Machocki, W. Grzegorczyk, A. Denis, Catal. Today 176 (2011) 14-20.

2 B. Banach, A. Machocki., P. Rybak, A. Denis, W. Grzegorczyk, W. Gac, Catal. Today 176 (2011) 28-35.

3 S.S.Y. Lin, D.H. Kim., S.Y. Ha, Catal. Lett. 122 (2008) 295-301.

4 I.I. Soykal, H.Sohn, U.S. Ozkan, ACS Catal. 2 (2012) 2335-2348.

5 S.-W. Yu, H.-H. Huang, C.-W. Tang, C.-B. Wang, Int. J. Hydrogen Energy 39 (2014) 20700-20711.

6 A.R. Passos, L. Martins, S.H. Pulcinelli, C.V. Santilli, V. Briois, Catal. Today 229 (2014) 88-94.

7 L. Óvári, S. Krick Calderon, Y. Lykhach, J. Libuda, A. Erdőhelyi, C. Papp, J. Kiss, H.-P. Steinrück, J. Catal. 307 (2013) 132-139.

8 F. Sadi, D. Duprez, F. Gerard, A. Miloudi, J. Catal. 213 (2003) 226-234.

9 T.X.T. Sayle, S.C. Parker, C.R.A. Catlow, Surf. Sci. 316 (1994) 329-336.

10 W. Xu, R. Si, S.D. Senanayake, J. Llorca, H. Idriss, D. Stacchiola, J.C. Hanson, J.A. Rodriguez, J. Catal. 291 (2012) 117-126.

11 R.J. Gorte, S. Zhao, Catal. Today 104 (2005) 18-24.

12 A. Machocki, A. Denis, W. Grzegorczyk, W. Gac, Appl. Surf. Sci. 256 (2010) 5551-5558.

13 H. Song, L. Zhang, U.S. Ozkan, Top. Catal. 55 (2012) 1324-1351.

14 H. Song, L. Zhang, U.S. Ozkan, Ind. Eng. Chem. Res. 49 (2010) 8984-8989.

15 H. Song, U.S. Ozkan, J. Mol. Catal. A 318 (2010) 21-29.

16 H. Song, B. Mirkelamoglu, U.S. Ozkan, Appl. Catal. A 382 (2010) 58-64.

17 H. Song, U.S. Ozkan, J. Catal. 261 (2009) 66-74.

18 H. Song, B. Tan, U.S. Ozkan, Catal Lett. 132 (2009) 422-429.

19 H. Wang, Y. Liu, L. Wang, Y.N. Qin, Chem. Eng. J. 145 (2008) 25-31.

20 A.S.P. Lovón, J.J. Lovón-Quintana, G.I. Almerindo, G.P. Valença, M.I.B. Bernardi, V.D. Araújo, T.S. Rodrigues, P.A. Robles-Dutenhefner, H.V. Fajardo, J. Power Sources 216 (2012) 281–289.

21 S.M. de Lima, A.M. Silva, U.M. Graham, G. Jacobs, B.H. Davis, L.V. Mattos, F.B. Noronha, Appl. Catal. A 352 (2009) 95-113.

22 A.M. da Silva, K.R. de Souza, L.V. Mattos, G. Jacobs, B.H. Davis, F.B. Noronha, Catal. Today 164 (2011) 234-239.

23 J. Llorca , P.R. de la Piscina, J.-Al. Dalmon, N. Homs, Chem. Mater. 16 (2004) 3573-3578.

24 S. Tuti, F. Pepe, Catal Lett. 122 (2008) 196-203.

25 V.A. de la Peña O'Shea, N. Homs, E.B. Pereira, R. Nafria, P.R. de la Piscina, Catal. Today 126 (2007) 148-152.

26 A.M. Karim, Y. Su, M.H. Engelhard, D.L. King, Y. Wang, ACS Catal. 1 (2011) 279-286.

27 J. Llorca, J.-A. Dalmon, P.R. de la Piscina, N. Homs, Appl. Catal. A 243 (2003) 261-269.

28 H. Song, L. Zhang, R.B. Watson, D. Braden, U.S. Ozkan, Catal. Today 129 (2007) 346-354.

29 M.S. Batista, R.K.S. Santos, E.M. Assaf, J.M. Assaf, E.A. Ticianelli, J. Pow. Sources 124 (2003) 99-103.

30 M.P. Hyman, J.M. Vohs, Surf. Sci. Lett. 605 (2011) 383-389.

31 Z. Ferencz, A. Erdőhelyi, K. Baán, A. Oszkó, L. Óvári, Z. Kónya, C. Pap, H.-P. Steinrüc, J. Kiss, ACS Catal. 4 (2014) 1205-1218.

32 T. Herranz, X. Deng, A. Cabot, J. Guo, M. Salmeron, J. Phys. Chem. B 113 (2009) 10721-10727.

33 E. Martono, J.M. Vohs, J. Catal. 291 (2012) 79-86.

34 B. Bayram, I.I. Soykal, D. von Deak, J.T. Miller, U.S. Ozkan, J. Catal. 284 (2011) 77-89.

35 V. Papaefthimiou, T. Dintzer, V. Dupuis, A. Tamion, F. Tournus, D. Teschner, M. Haevecker, A. Knop-Gericke, R. Schloegl, S. Zafeiratos, J. Phys. Chem. Lett., 2 (2011) 900-904.

36 S. Zafeiratos, T. Dintzer., D. Teschner, R. Blume, M. Hävecker, A. Knop-Gericke, R. Schlögl, J. Catal. 269 (2010) 309-317.

37 A. Tuxen, S. Carenco, M. Chintapalli, C.-H. Chuang, C. Escudero, E. Pach, P. Jiang, F. Borondics, B. Beberwyck, A. Paul Alivisatos, G. Thornton, W.-F. Pong, J. Guo, R. Perez, F Besenbacher, M. Salmeron, J. Am. Chem. Soc. 135 (2013) 2273-2278.

38 V. Papaefthimiou, T. Dintzer, V. Dupuis, A. Tamion, F. Tournus, A. Hillion, D. Teschner, M. Hävecker, A. Knop-Gericke, R. Schlögl, S. Zafeiratos, ACS Nano 5 (2011) 2182-2190.

39 S.C. Petitto, E.M. Marsh, G.A. Carson, M.A. Langell, J. Mol. Catal. A 281 (2008) 49-58.

40 M.C. Biesinger, B.P. Payne, A.P. Grosvenor, L.W.M. Laum A. R. Gerson, R.St.C. Smart, Appl. Surf. Sci. 257 (2011) 2717-2730.

41 W. Xu, Z. Liu, A.C. Johnston-Peck, S.D. Senanayake, G. Zhou, D. Stacchiola, E.A. Stach, J.A. Rodriguez, ACS Catal. 3 (2013) 975-978.

42 V. Papaefthimiou, M. Shishkin, D.K. Niakolas, M. Athanasiou, Y.T.Law, R. Arrigo, D. Teschner, M. Hävecker, A. Knop-Gericke, R. Schlögl, T. Ziegler, S.G. Neophytides, S. Zafeiratos, Adv. Energy Mater. 3 (2013) 762–769.

43 C. Padeste, N.W. Cant, D.L. Trimm., Catal Lett. 24 (1994) 95-105.

44 L. Qiu, F. Liu, L. Zhao, Y. Ma, J. Yao, Appl. Surf. Sci. A 252 (2006) 4931-4935.

45 E. Paparazzo, Surf. Sci. Lett. 234 (1990) 253-259.

46 D.A. Creaser, P.G. Harrison, Catal Lett. 23 (1994) 13-24.

47 B.E. Koel, G. Praline, H.-I. Lee, J.M. White, R.L. Hance, J. Electron. Spectrosc. Relat. Phenom. 21 (1980) 31-46.

48 Y. Wu, J.T. Mayer, E. Garfunkel, T.E. Madey, Langmuir 10 (1994) 1482-1487.

49 A. Pfau, K.D. Schierbaum, Surf. Sci. 321 (1994) 71-80.

50 J.P. Holgado, G. Munuera, J.P. Espinós, A.R. González-Elipe, Appl. Surf. Sci. 158 (2000) 164-171.

51 T.-L. Chen, D.R. Mullins, J. Phys. Chem. C 115 (2011) 3385-3392.

52 M. Nagai, R. Isoe, K. Ishiguro, H. Tominaga, M. Shimizu, Chem. Eng. J. 207 (2012) 938-942.

53 J. Światowska, V. Lair, C. Pereira-Nabais, G. Cote, P. Marcus, A. Chagnes, Appl. Surf. Sci. 257 (2011) 9110-9119.

54 D. Rosenthal, M. Ruta, R. Schlögl, L. Kiwi-Minsker, Carbon 48 (2010) 1835-1843.

55 W. Luo, A. Asthagiri, Catal. Sci. Technol. 4 (2014) 3379-3389.

56 H. Song, L. Zhang, U.S. Ozkan, Green Chem. 9 (2007) 686-694.

57 A. Bshish, Z. Yakoob, B. Narayanan, R. Ramakrishnan, A. Ebshish, Chem Papers 65 (2011) 251-266.

58 L.V. Mattos, G. Jacobs, B.H. Davis, F.B. Noronha, Chem. Rev. 112 (2012) 4094-4123.
59 R. M. Ferrizz, G. S. Wong, T. Egam, J. M. Vohs, Langmuir 17 (2001) 2464–2470.
60 A. Yee, S.J. Morrison, H. Idriss, J. Catal. 191 (2000) 30-45.
61 A.M. da Silva, K.R. de Souza, G. Jacobs, U.M. Graham, B.H. Davis, L.V. Mattos, F.B. Noronha, Appl. Catal. B 102 (2011) 94-109.
62 I.I. Soykal, H. Sohn, D. Singh, J.T. Miller, U.S. Ozkan, ASC Catal. 4 (2014) 585-592.
63 S.M. de Lima, A.M. da Silva, L.O.O. da Costa, U.M. Graham, G. Jacobs, B.H. Davis, L.V. Mattos, F.B. Noronha, J. Catal 268 (2009) 268-281.
64 J.M. Sun, D.H. Mei, A.M. Karim, A.K. Datye, Y. Wang, ChemCatChem 5 (2013) 1299–1303.
65 E. Martono, J.M. Vohs, ASC Catal. 1 (2011) 1414–1420.
66 E. Varga, Z. Ferencz., A. Oszkó, A. Erdöhelyi, J. Kiss, J. Mol. Catal. A 397 (2015) 127-133.
67 S.S.-Y. Lin, D.H.K., S.Y. Ha, Appl. Catal. A 355 (2009) 69-77.
68 N. Laosiripojana, S. Assabumrungrat, Appl. Catal. B 66 (2006) 29-39.
69 S.M. de Lima, A.M. Silva, I.O. da Cruz, G. Jacobs, B.H. Davis, L.V. Mattos, F.B. Noronha, Catal. Today 138 (2008) 162-168.
70 L.del Río, I. López, G. Marbán, Appl. Catal. B 150–151 (2014) 370–379.
71 T.-L. Chen and D. R. Mullins, J. Phys. Chem. C 115 (2011) 3385–3392.
72 R. Padilla, M. Benito, L. Rodríguez, A. Serrano, G. Muñoz, L. Daza, Int. J. Hydrogen Energy 35 (2010) 8921-8928.
73 D. Zanchet, J.B.O. Santos, S. Damyanova, J.M.R. Gallo, J.M.C. Bueno, ASC Catal. 5 (2015) 3841-3863.
74 E. Martono, M.P. Hyman, J.M. Vohs, Phys. Chem. Chem. Phys. 13 (2011) 9880-9886.
75 D.R. Mullins, P.M. Albrecht, J. Phys. Chem. C 117 (2013) 14692-14700.
76 C.N. de Ávila, C.E. Hori, A.J. de Assis, Energy 36 (2011) 4385-4395.